Published in final edited form as:
Vet Radiol Ultrasound. 2011 ; 52(4): 362–367. doi:10.1111/j.1740-8261.2011.01822.x.

PULMONARY ANGIOGRAPHY WITH 64-MULTIDETECTOR-ROW COMPUTED TOMOGRAPHY IN NORMAL DOGS

Randi Drees, **Alex Frydrychowicz**, **Nicholas S. Keuler**, **Scott B. Reeder**, and **Rebecca Johnson**
Department of Surgical Sciences, School of Veterinary Medicine, University of Wisconsin-Madison, Linden Drive 2015, Madison, WI 53706 (Drees, Johnson), Department of Radiology (Frydrychowicz, Reeder), Medical Physics (Reeder), Biomedical Engineering and Medicine (Reeder), School of Medicine and Public Health, University of Wisconsin-Madison, 600 Highland Avenue, Madison, WI 53792, and Department of Statistics (Keuler), University of Wisconsin-Madison, 1300 University Avenue, Madison, WI 53706

Abstract

Pulmonary angiography using 64-multidetector-row computed tomography (MDCT) was used to evaluate pulmonary artery anatomy, and determine the sensitivity of pulmonary artery segment visualization in four Beagle dogs using images reconstructed to 0.625 mm and retro-reconstructed to 1.25 and 2.5 mm slice thickness. Morphologically, characteristic features included a focal narrowing in the right cranial pulmonary artery in all dogs, which should not be mistaken as stenosis. While the right cranial pulmonary artery divided into two equally sized branches that were tracked into the periphery of the lung lobe in all dogs, only a single left cranial (cranial portion) lobar artery was present. Compared with 1.25 and 2.5 mm retro-reconstructions, 0.625 mm reconstructions allowed for detection of significantly ($P \leq 0.05$) more pulmonary artery segments and sharper depiction of vessel margins. Clinical applications such as prevalence and significance of diameter changes, and detection of pulmonary arterial thrombembolism on lobar and sublobar level, using pulmonary angiography with 64-MDCT applying 0.625 mm reconstruction slice thickness remain to be established.

Keywords

canine; lung; multidetector computed tomography; pulmonary artery

Introduction

Diagnostic imaging evaluation of the pulmonary arteries in dogs is based mainly on thoracic radiographs, though in some patients more specific procedures such as angiography or scintigraphy are conducted.[1,2] All of these methods are limited by morphological accuracy, and some also by invasiveness. Multidetector-row computed tomography (MDCT) pulmonary angiography is the standard of care for diagnosing pulmonary embolism in humans.[3–6] There is only limited information on MDCT pulmonary angiography in dogs.[7–11] Therefore, our goal was to evaluate normal canine pulmonary arteries using 64-MDCT.

Address correspondence and reprint requests to Dr. Randi Drees, at the above address. drees@svm.vetmed.wisc.edu.

Material and Methods

General anesthesia was induced in four 1-year-old Beagle dogs (mean body weight 11 ± 0.5 kg) with propofol* and maintained with isoflurane in 100% oxygen administered via an orotracheal tube. End-tidal carbon dioxide levels were kept between 35–45 mmHg using a mechanical ventilator.† Intravenous crystalloid solution‡ was administered though a 22 G catheter in the left cephalic vein at 10 ml/kg/h with fluid boluses of 5 ml/kg as necessary to maintain blood pressure. Esmolol (50–300 mg/kg/min) was also administered through this catheter as part of a separate study of coronary angiography.

Dogs were in dorsal recumbency using a V-trough on a clinical 64-multidetector-row computed tomography scanner§. A 20 G catheter was placed in the right cephalic vein for contrast medium injection. The arrival time of contrast medium was determined using a test bolus approach: A bolus of 5 ml iodinated contrast medium¶ followed by a 20 ml saline chaser was injected at 2 ml/s within maximum pressure limits of 300 lb/in^2 with a dual barrel power injector.‖ After injection, repetitive transverse plane cine scans (80 kV, 40 mA, 5 mm slice thickness, axial scanning mode, 1-s tube rotation time, one image acquired per rotation) were acquired over the mediastinum transecting the base of the main pulmonary artery (MPA) and aorta. Time to peak enhancement in the MPA and aorta was analyzed on the scanner by placement of a region of interest (ROI) in the center of the respective vessel.

The study bolus time was set to allow for simultaneous pulmonary arterial and aortic opacification for a related project. A triphasic injection protocol was used with an initial bolus consisting of 100% contrast medium, followed by dilute contrast medium (40–60% physiologic saline solution), and a terminal saline chaser. In total, 2.4–3.9 ml contrast medium/kg bodyweight were administered using an identical injection speed as that used for the test bolus.

Following a 4-s delay from peak enhancement at the aortic root, the thorax was scanned in caudocranial direction, with the scan field of view (FOV) adapted to each dog's individual anatomy including both pulmonary apices and all costophrenic recesses. The extended and triphasic bolus was chosen to allow opacification of the pulmonary arteries as well as all chambers and great vessels for a related project. Imaging settings were: helical scan mode at 120kV tube voltage, ECG-modulated tube current (200–750 mA), 0.35 s tube rotation time (effective temporal resolution 250 ms using SnapShot Segment feature, proprietary**), prospective ECG-gating with heart-rate adapted pitch, 64 × 0.625 mm collimation (i.e., using 64 detector rows of 0.625 mm width) was applied for all studies. Images were reconstructed to isotropic 0.625 mm and retro-reconstructed to nonisotropic 1.25 and 2.5 mm slice thickness using a soft tissue kernel. All dogs were euthanized following a related coronary angiography study and underwent necropsy examination.

Image evaluation was performed by a board certified veterinary radiologist on a dedicated viewing station OsiriX® Medical Image software, version 3.7.1 (http://www.osirix-viewer.com/). The studies were randomized and anonymized so that the reviewer was not aware of the specific reconstruction algorithm. For evaluation of images, window width and level were adjusted individually to optimize visualization of the pulmonary arteries.

*PropoFlo™, Abbott Laboratories, North Chicago, IL.
†SAV 2500, Smiths Medical, Waukesha, WI.
‡Plasma-lyte A, Baxter Healthcare Corporation, Deerfield, IL.
§VCT, GE Healthcare, Waukesha, WI.
¶Isovue 370, Bracco Diagnostics Inc., Princeton, NJ.
‖Stellant, MedRad, Indianola, PA.
**GE Healthcare.

Enhancement levels of the main (MPA), main right (RPA), main left pulmonary (LPA) artery, and aorta were measured on 0.625 mm reconstructed images by manually placing regions of interest (ROIs) in comparable regions of the respective vessels; the thinnest slice thickness allowing for the most accurate anatomical placement of the ROI.

The pulmonary arterial vessels (MPA, RPA, LPA, right cranial, middle, caudal and accessory, left cranial (cranial portion), cranial (caudal portion), and caudal pulmonary arterial lobar branches) were evaluated further using all three reconstruction thicknesses for the following criteria: (1) anatomy: relationship to major vessels, cardiac, and visible bronchial structures were qualitatively recorded; and (2) detectable lobar arterial segments: starting with the most proximal segment of the individual lobar artery, the vessel was followed distally, each point of subdivision into smaller branches marking the beginning of a new segment.

The effect of the reconstruction interval on the number of detectable segments was analyzed for each lobe separately using repeated measures ANOVA with an autoregressive correlation structure within dogs. If the overall *F*-test was significant, pair-wise comparisons of different reconstruction thicknesses were done using the Tukey multiple comparisons adjustment separately for each lobe. All analyses were done in Proc Mixed using SAS 9.2 for Windows.[12] The significance level was set at $P \leq 0.05$.

Results

Pulmonary angiography was performed successfully in all animals. The FOV was adjusted to the individual anatomy and extended 19.2, 22.5, 19.3, and 20.2 cm in craniocaudal direction in each of the four dogs. On subsequent necropsy examination, the pulmonary arteries were within normal limits and no thrombi were found.

Results for time to peak enhancement after test bolus, individualized study bolus volumes, and enhancement after injection of study bolus are summarized in Table 1. Adjusting scan delay for the inter-individual temporal variability determined from test bolus arrival produced good enhancement of >300 HU in the pulmonary arteries and aorta in all dogs.

Figure 1 shows volume rendered images allowing for a morphologic overview of the anatomic relationship of the major cardiovascular structures. On transverse and multiplanar reconstructions the pulmonic cusps were outlined faintly and the pulmonic bulb was seen distinctly on 0.625 mm reconstructed images, whereas on 1.25 and 2.5 mm retro-reconstructions, the cusps are indistinct or not visible and the outline of the pulmonic bulb was mild to very indistinct, respectively (Fig. 2). The MPA arose from the RVOT left of midline in a craniodorsal direction flanked by the tip of the left atrial (LA) appendage laterally and the ascending aorta (AO) medially. The bifurcation of the MPA into the LPA and RPA occurred dorsal to the aortic root and left ventrally to the carina (see also Fig. 1).

The RPA proceeded in the dorsal plane laterally towards the right, the right cranial lobar artery branched straight laterally from its cranial aspect. A smooth dorsoventral focal narrowing of the right cranial lobar artery was observed in all dogs, which can be attributed to the passage between trachea and right atrium. On 1.25 and 2.5 mm retro-reconstructions, a decrease in diameter could be seen on one side of the right cranial lobar artery but not a focal narrowing. The right cranial lobar artery then continued cranioventrally, pivoting over the right cranial lobar bronchus, undergoing bifurcation as it crossed caudally to the right azygos vein and cranially to the right cranial lobar bronchus. Both branches ran in the cranial direction, one in a more dorsal plane extending into the craniodorsal portion of the right cranial lung lobe without crossing the midline. The second branch extended in a more

ventral plane into the cranioventral tip of the right cranial lobe, crossing the midline to the left.

The RPA ran in the caudolateral direction, crossing dorsally to the right caudal pulmonary vein and ventral to the right main stem bronchus. It continued along the ventrolateral aspect of the right bronchus. At the respective lobar bronchial divisions, the right middle lobar artery originated ventrolaterally; immediately caudally the accessory lobar artery branched ventromedially. The right caudal lobar artery continued in the caudodorsal direction.

The LPA traversed dorsal to the LA appendage and left cranial pulmonary vein and ventrally to the descending aorta describing a caudodorsal curve. The left cranial lobar artery (cranial portion) exited ventrolaterally, curving over the cranial lobar bronchus (cranial portion). The LPA then passed dorsally to the main left lobar bronchus, which had a mild indentation at that level. The PA branch to the caudal portion of the left cranial lung lobe exited in ventrolateral direction at the level of its lobar bronchus. The left caudal pulmonary artery continued in the caudodorsal direction. All lobar pulmonary arteries followed laterally adjacent to their respective bronchi into the periphery, medium sized to very small sublobar artery branches arose in a dichotomous or trichotomous fashion, most commonly at the level of lobar bronchial divisions.

The MPA, RPA, LPA, and all lobar pulmonary arteries were visible on images of all three collimations. Mild to moderate blur of the vessel margins was seen on images retro-reconstructed to 1.25 and 2.5 mm, whereas vessel margins were sharp on images reconstructed to 0.625 mm slice thickness (Fig. 3).

The range of detected segments in the lobar arteries was 12–19 segments on 0.625 mm reconstructions, 8–14 segments on 1.25 mm, 7–11 on 2.5 mm retro-reconstructions. Detailed results of recorded segments of the individual lobar arteries are given in Fig. 4.

There were significant differences ($P \leq 0.05$) of visible segments between all reconstruction thicknesses in the right cranial (vent) and right accessory lobar arteries. In the right cranial (dors), right middle, and right caudal lobar artery significantly ($P \leq 0.05$) more segments could be seen on 0.625 mm reconstructed images compared with both larger retro-reconstruction thicknesses. For the all three left lobar arteries, there were significant differences ($P \leq 0.05$) between 0.625 mm and both larger retro-reconstruction thicknesses.

Discussion

Pulmonary angiography with 64-MDCT depicted the anatomy of the canine pulmonary arterial tree in vivo as described in the literature.[13–15] Understanding the pulmonary arterial anatomy and knowledge of normal variants is essential for clinical evaluation in a variety of diseases.

Even though pulmonic stenoses are observed most commonly at valvular, supravalvular, or subvalvular levels,[16] peripheral pulmonary artery stenosis has been described.[17] A focal narrowing in diameter of the right cranial lobar artery was detected in all dogs and this should not be mistaken for a stenosis. The right cranial lobar artery is the first branch of the right pulmonary artery, exiting straight laterally. When viewing in the transverse plane only, care must be applied to evaluate the right cranial lobar artery separately from the continuation of the right pulmonary artery that can be seen just caudally. The left pulmonary artery causes a focal indentation in the bronchial lumen as it passes dorsal to the left main stem bronchus, considered a normal variant. Compression of the left main stem bronchus is described on lateral radiographs in dogs with an enlarged left atrium.[18] In contrast, the right pulmonary artery passes ventral to the respective bronchus and does not cause a narrowing.

Interestingly, two similar sized lobar vessels were seen in all right cranial lung lobes, whereas a single right cranial lobar vessel is usually described.[13,14]

As only a small number of dogs of the same breed were used in this study, what has been described as anatomic variations, has to be considered with care and may not be transferred to other breeds.

Mild and mild-moderate blurring of vascular margins was observed using 1.25 and 2.5 mm retro-reconstructed slice thickness, attributable to partial volume effects.[19] However, decreased image noise in reconstructed slice thickness greater than 0.625 mm gives the images a more smooth and flat appearance.[20] Another trade-off between appearance and spatial resolution is that fewer generations of sublobar branches were detected on 1.25 and 2.5 mm retro-reconstruction thicknesses; these were branches in the <1 mm range. Also note that nonisotropic slice-thickness can lead to decreased image analysis capabilities using multiplanar reformats.

A metaanalysis on pulmonary single detector CTA (SD-CTA) with suboptimal 5 mm sections[21] led the American College of Chest Physicians and the American Thoracic Society to conclude that pulmonary SD-CTA was an insufficient clinical test to exclude pulmonary embolism in people. Reducing the collimation in pulmonary SD-CTA from 3 to 2 mm, however, increases the percentage of visualized subsegmental arteries.[22,23] Also, significant improvement of sensitivity regarding subsegmental pulmonary embolism was reported comparing 3 mm pulmonary SD-CTA to 2.5 and 1.25 mm multidetector row pulmonary CTA in people, the latter increasing the sensitivity.[24] Clinical relevance of subsegmental emboli is uncertain in both people and animals.[25,26] On the other hand, diseases such as pulmonary hypertension can affect the appearance of the small sublobar arteries in pulmonary CTA. While this is established in people,[27] this has not been investigated in animals.

Scan timing in relation to contrast medium injection is crucial for successful opacification of the pulmonary arteries or other vascular structures. To achieve this goal, various techniques can be applied. Fixed delay/best guess approaches, test bolus, and bolus tracking methods have been used previously in people[28–30] and dogs.[8,10,11,31] Bolus tracking methods are efficient and practical as the bolus for the diagnostic study is used to trigger the scan. Our test bolus method requires two injections (test and diagnostic bolus), thereby increasing the dose of contrast medium and fluid volume. However, it provides additional testing of the integrity of the venous access system and was used in our study as it is the preferred method in our institution. Potential hemodynamic effects, which were not considered during our study, could be overcome by the use of smaller, potentially weight- or body surface area-adapted injection volumes.

Similarly, the alternative of a fixed scan delay on the order of 15–25 s have given adequate results in pulmonary CTA in humans because the contrast enhancement rises rapidly with fast injections in the pulmonary arteries. However, patient dependent factors such as cardiac output and the related contrast medium transit time may delay enhancement significantly and lead to suboptimal timing. Subsequent insufficient contrast enhancement might cause the need for repeated studies.

Individualized scan delays using test bolus or bolus tracking approaches are designed to overcome such potential sources of error.[29,32] The test bolus technique is applied routinely in clinical practice and was used in our study.[31,32,33] Time of contrast medium arrival in the pulmonary artery in our study was similar to previous work.[8,10] The prolonged injection duration and correlating high contrast medium volumes were chosen to allow for pulmonary arterial, systemic arterial, as well as all cardiac chamber opacification for a related project.

Hence, described injection bolus volume is larger than necessary for only canine pulmonary CTA.

Reports on minimum or maximum enhancement levels needed for diagnostic CT angiography are sparse. Estimated values of the minimal enhancement range from 250 to 350 HU (i.e. attenuation of 300–400 HU).[29,33] We obtained higher enhancement values that can therefore be considered diagnostic.

In summary, pulmonary angiography using 64-MDCT enables visualization of the canine pulmonary arterial anatomy in vivo. Using slice thickness greater than 0.625 mm decreases the number of visible lobar artery segments and induces blurring of vascular margins. The right cranial pulmonary artery has a focal indentation that should not be mistaken for a stenosis.

Acknowledgments

This project was funded by the Companion Animal Fund of the University of Wisconsin-Madison. Rebecca Johnson is supported by Grant 1UL1RR025011 from the Clinical and Translational Science Award (CTSA) program of the National Center for Research Resources (NCRR), National Institutes of Health (NIH).

REFERENCES

1. Myer C. Radiographic review: the vascular and bronchial patterns of pulmonary disease. Vet Radiol. 1980; 21:156–160.
2. Koblik PD, Hornof W, Harnagel SH, Fisher PE. A comparison of pulmonary angiography, digital subtraction angiography, and 99mTc-DTPA/MAA ventilation-perfusion scintigraphy for detection of experimental pulmonary emboli in the dog. Vet Radiol. 1989; 30:159–168.
3. Remy-Jardin M, Remy J. Vascular disease in chronic obstructive pulmonary disease. Proc Am Thorac Soc. 2008; 5:891–899. [PubMed: 19056712]
4. Lee KS, Bae WK, Lee BH, Kim IY, Choi EW. Bronchovascular anatomy of the upper lobes: evaluation with thin-section CT. Radiology. 1991; 181:765–772. [PubMed: 1947094]
5. Cummings K, Bhalla S. Multidetector computed tomographic pulmonary angiography: beyond acute pulmonary embolism. Radiol Clin North Am. 2010; 48:51–65. [PubMed: 19995629]
6. Jardin M, Remy J. Segmental bronchovascular anatomy of the lower lobes: CT analysis. Am J Roentgenol. 1986; 147:457–468. [PubMed: 3488646]
7. Lee CH, Goo JM, Bae KT, et al. CTA contrast enhancement of the aorta and pulmonary artery: the effect of saline chase injected at two different rates in a canine experimental model. Invest Radiol. 2007; 42:486–490. [PubMed: 17568270]
8. Makara M, Glaus T, Dennler M, et al. Multi-row computed tomography angiography technique of the canine pulmonary vasculature. Vet Radiol Ultrasound. 2010; 51:232.
9. Takahashi A, Yamada K, Kishimoto M, Shimizu J, Maeda R. Computed tomography (CT) observation of pulmonary emboli caused by long-term administration of ivermectin in dogs experimentally infected with heartworms. Vet Parasitol. 2008; 155:242–248. [PubMed: 18602759]
10. Habig A, Beal M, Brown A, Nelwon N, Coehlo J, Kinns J. Pulmonary angiography using 16 slice multidetector computed tomography in clinically normal dogs. Vet Radiol Ultrasound. 2010; 51:232.
11. Seiler GS, Nolan TJ, Withnall E, Reynolds C, Lok JB, Sleeper MM. Computed tomographic changes associated with the prepatent and early patent phase of dirofilariasis in an experimentally infected dog. Vet Radiol Ultrasound. 2010; 51:136–140. [PubMed: 20402396]
12. SAS/STAT Software. Version 9.2 of the SAS System for Windows. Cary, NC: Copyright© 2009 SAS Institute Inc. SAS and all other SAS Institute Inc. product or service names are registered trademarks or trademarks of SAS Institute Inc.;
13. Evans, HE. The pulmonary arteries and veins. In: Evans, HE., editor. Miller's anatomy of the dog. Philadelphia: Saunders; 1993. p. 601-602.

14. Koch, T.; Berg, R. Arterien des kleinen oder Lungenkreislaufs. In: Berg, R., editor. Lehrbuch der Veterinaer-Anatomie. Stuttgart: Gustav Fischer Verlag; 1993. p. 44-45.
15. Koenig, H.; Liebich, HG. Der Atmungsapparat (Apparatus respiratorius). Anatomie der Haussaeugetiere. Stuttgart: Schattauer GmbH; 2005. p. 388
16. Oyama, MADS.; Thomas, WP.; Bonagura, JD. Congenital heart disease. In: Ettinger, SJ.; Feldman, EC., editors. Textbook of veterinary internal medicine. St. Louis: Elsevier; 2005. p. 972-1021.
17. MacGregor JM, Winter MD, Keating J, Tidwell AS, Brown DJ. Peripheral pulmonary artery stenosis in a four-month-old West Highland White Terrier. Vet Radiol Ultrasound. 2006; 47:345–350. [PubMed: 16863051]
18. Bahr, RJ. Heart and pulmonary vessels. In: Thrall, DE., editor. Textbook of veterinary diagnostic radiology. St. Louis: Saunders Elsevier; 2007. p. 570-571.
19. Bushberg, JT.; Seibert, JA.; Lediholdt, EM., Jr; Boone, JM. Computed tomography. In: Bushberg, JT., editor. The essential physics of medical imaging. Philadelphia: Lippincott Williams & Wilkins; 2002. p. 371-372.
20. Bushberg, JT.; Seibert, JA.; Lediholdt, EM., Jr; Boone, JM. Computed tomography. In: Bushberg, JT., editor. The essentials of physics of medical imaging. Philadelphia: Lippincott Williams & Wilkins; 2002. p. 367-369.
21. Rathbun SW, Raskob GE, Whitsett TL. Sensitivity and specificity of helical computed tomography in the diagnosis of pulmonary embolism: a systematic review. Ann Intern Med. 2000; 132:227–232. [PubMed: 10651604]
22. Remy-Jardin M, Remy J, Artaud D, Deschildre F, Duhamel A. Peripheral pulmonary arteries: optimization of the spiral CT acquisition protocol. Radiology. 1997; 204:157–163. [PubMed: 9205239]
23. Remy-Jardin M, Baghaie F, Bonnel F, Masson P, Duhamel A, Remy J. Thoracic helical CT: influence of subsecond scan time and thin collimation on evaluation of peripheral pulmonary arteries. Eur Radiol. 2000; 10:1297–1303. [PubMed: 10939495]
24. Patel S, Kazerooni EA, Cascade PN. Pulmonary embolism: optimization of small pulmonary artery visualization at multi-detector row CT. Radiology. 2003; 227:455–460. [PubMed: 12732699]
25. Le Gal G, Righini M, Parent F, van Strijen M, Couturaud F. Diagnosis and management of subsegmental pulmonary embolism. J Thromb Haemost. 2006; 4:724–731. [PubMed: 16634736]
26. MacDonald, KA.; Johnson, LR. Pulmonary hypertension and pulmonary thrombembolism. St. Louis: Elsevier; 2005. p. 1284-1288.
27. Cummings KW, Bhalla S. Multidetector computed tomographic pulmonary angiography: beyond acute pulmonary embolism. Radiol Clin North Am. 48:51–65. [PubMed: 19995629]
28. Bae KT. Optimization of contrast enhancement in thoracic MDCT. Radiol Clin North Am. 48:9–29. [PubMed: 19995627]
29. Bae KT, Heiken JP. Scan and contrast administration principles of MDCT. Eur Radiol. 2005; 15(Suppl 5):E46–E59. [PubMed: 18637230]
30. Cademartiri F, Nieman K, van der Lugt A, et al. Intravenous contrast material administration at 16-detector row helical CT coronary angiography: test bolus versus bolus-tracking technique. Radiology. 2004; 233:817–823. [PubMed: 15516601]
31. Jung J, Chang J, Oh S, Yoon J, Choi M. Computed tomography angiography for evaluation of pulmonary embolism in an experimental model and heartworm infested dogs. Vet Radiol Ultrasound. 2010; 51:288–293. [PubMed: 20469550]
32. Kuriakose J, Patel S. Acute pulmonary embolism. Radiol Clin North Am. 2009; 48:31–50. [PubMed: 19995628]
33. Wittram C. How I do it: CT pulmonary angiography. Am J Roentgenol. 2007; 188:1255–1261. [PubMed: 17449768]

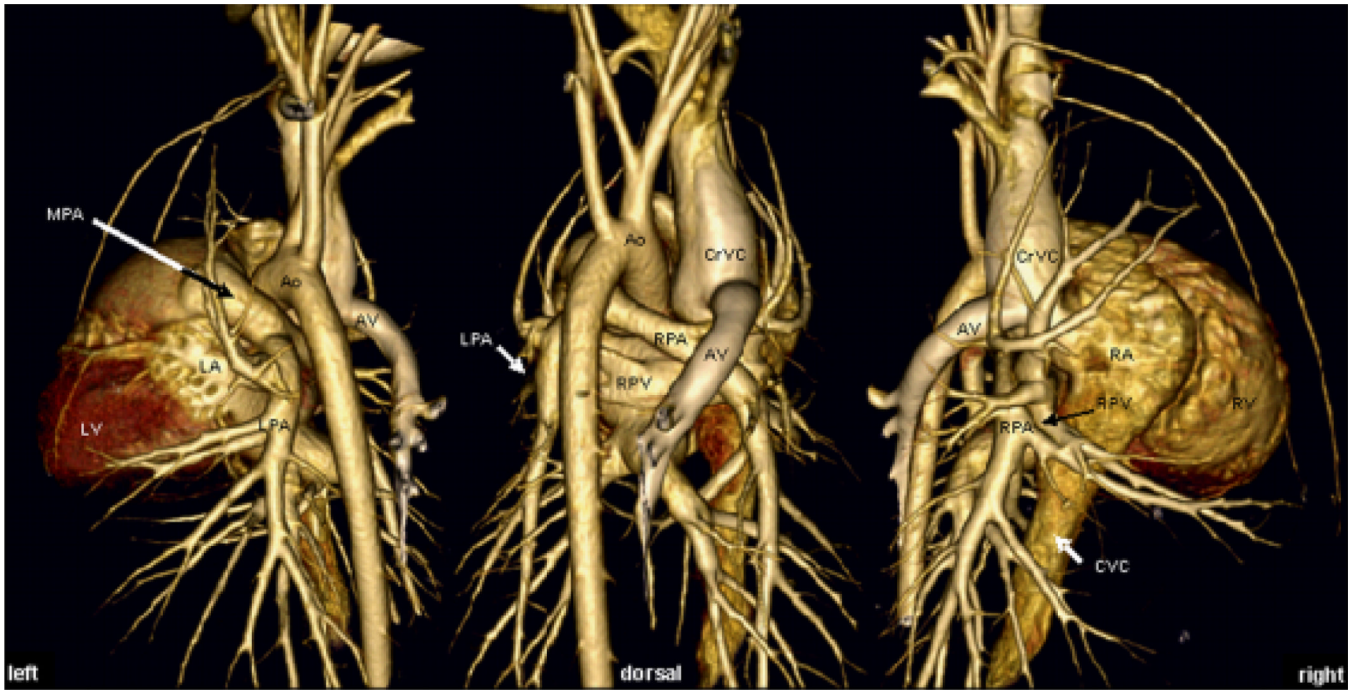

Fig. 1.

Volume rendered display of a representative dataset with 0.625 mm collimation. Although volume rendered displays were not part of the analysis, the ability to depict the anatomy was exploited for a morphologic overview over anatomic relationships of the major cardiovascular structures that have not been reported systematically and only presented sparsely in the literature. Note the straight lateral branching of the right cranial lobar artery and the continuation as two equally sized separate branches into the right cranial lung lobe on dorsal and right oblique image. MPA, main pulmonary artery; LPA, RPA, left and right main pulmonary artery, respectively; RPV, right pulmonary vein; CrVC, cranial vena cava; CVC, caudal vena cava; LV, RV, left and right ventricle, respectively; LA, RA, left and right atrium, respectively; AV, right azygos vein.

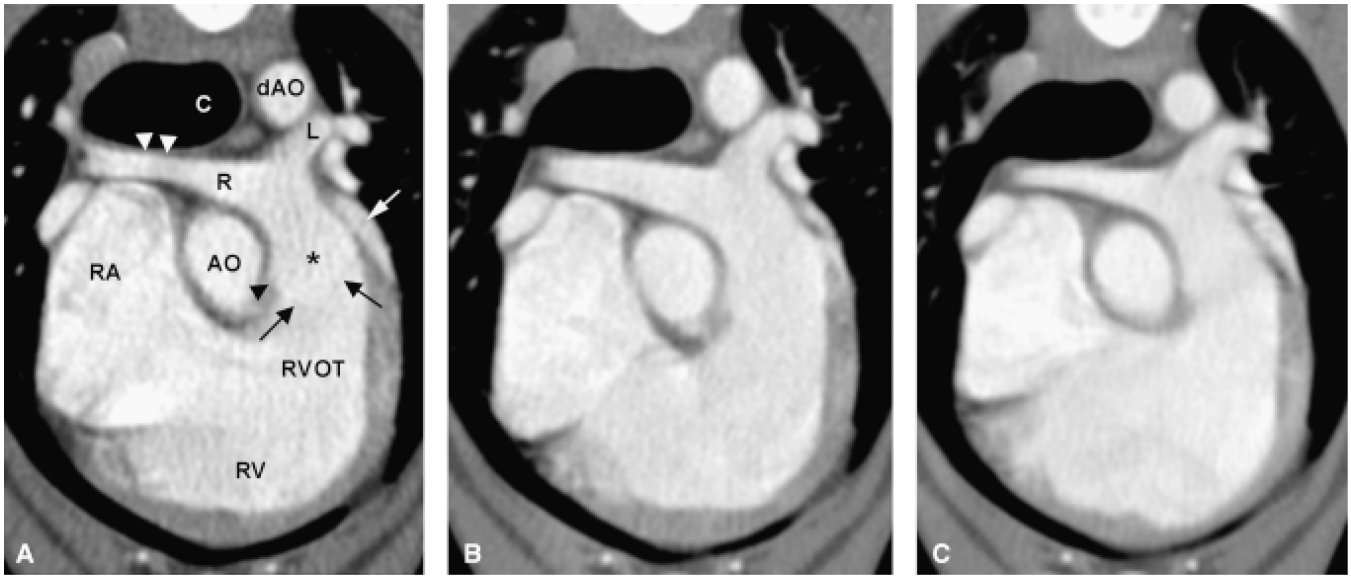

Fig. 2.

Transverse view of right ventricular outflow tract, main pulmonary artery and its left and right branches and comparison of three collimation settings. Transverse plane reconstruction of 0.625 mm (A) and retro-reconstruction of 1.25 mm (B), and 2.5 mm (C) slice thickness. The main pulmonary artery (*) arises from the right ventricular outflow tract (RVOT) left of midline in a craniodorsal direction flanked by the tip of the left atrial appendage (white arrow) laterally and the ascending aorta (AO) medially. Only on 0.625 mm reconstruction the fine outline of the cusp (black arrows) can be seen, also on the larger retro-reconstructions, the pulmonic bulb (black arrow head) is less distinct. The right cranial lobar artery has a smooth dorsoventral focal narrowing (white arrowheads) as it passes ventral to the trachea dorsally to the right atrium. L, R, left and right pulmonary artery, respectively; C, carina; dAO, descending aorta; RA, right atrium; RV, right ventricle.

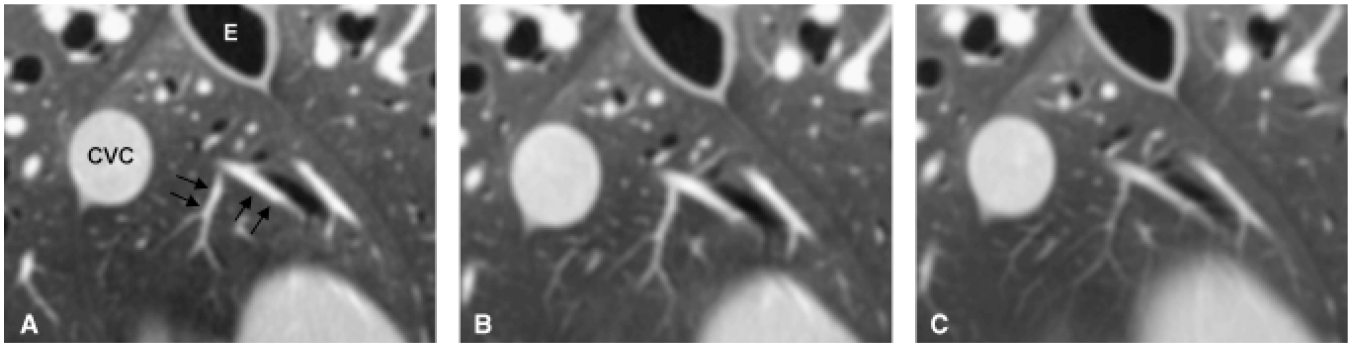

Fig. 3.

Visualization of pulmonary artery branches and segments using three different reconstruction slice thicknesses. Pulmonary artery branches (black arrows) in the accessory lung lobe on 0.625 mm reconstruction (A), 1.25 mm (B), and 2.5 mm (C) retro-reconstruction slice thickness. At 0.625 mm the vessel margins are sharp whereas at the larger retro-reconstruction slice thicknesses vessel margins are mild to moderately blurred and the image is smoother and flatter due to partial volume artifact. CVC, caudal vena cava; E, esophagus.

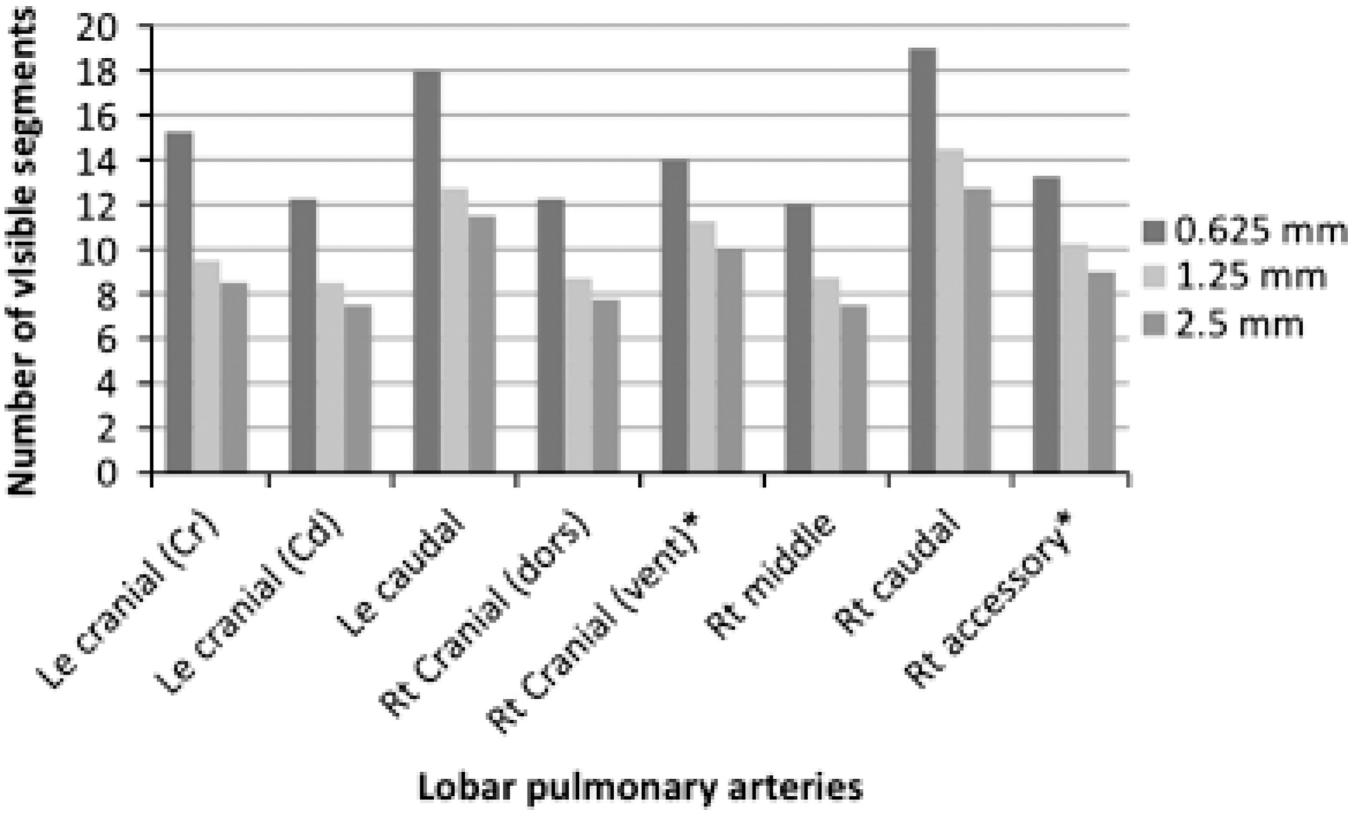

Fig. 4.

Averages of visible segments of the lobar pulmonary arteries based on reconstruction slice thickness. Significant differences (*) in the number of visible pulmonary arterial segments were found between all reconstruction thicknesses for the right cranial (vent) and accessory lobar arteries ($P \leq 0.05$). In all other lobar arteries significant differences in the number of visible pulmonary arterial segments were found on 0.625 mm reconstruction compared to both larger retro-reconstruction slice thicknesses ($P \leq 0.05$), and no significant difference was present between 1.25 and 2.5 mm retro-reconstructions ($P \geq 0.05$). Standard error for the estimated averages of visible segments of the lobar pulmonary arteries for all reconstruction thicknesses was 0.89 for the right cranial (dors), 0.58 for the right cranial (vent), 0.57 for the right middle, 0.98 for the right caudal, 0.92 for the right accessory, 0.74 for the left cranial (Cr), 1.52 for the left cranial (Cd), and 1.23 for the left caudal lobar artery.

Table 1

Time to Peak Enhancement, Study Bolus, and Enhancement Evaluation of the Pulmonary CTA in Four Dogs

	Time to Peak Enhancement After Test Bolus (s)			Enhancement After Study Bolus (HU [SD])	
	MPA	AO	Study Bolus (ml)*	MPA	AO
Dog 1	4	8	22/22/16	385.4 (15.9)	406.9 (19.3)
Dog 2	4	9	24/24/20	301.0 (16.9)	359.1 (20.0)
Dog 3	4	6	18/18/16	321.1 (20.6)	327.7 (18.4)
Dog 4	6	11	30/30/19	486.7 (18.7)	502.8 (18.3)

*100% iodinated contrast medium/40%/60% iodinated contrast medium/physiologic saline solution)/100% physiologic saline solution. MPA, main pulmonary artery; AO, ascending aorta.